

## Numerical Simulation of Air-Liquid Two-Phase Flow in Air-Layer Drag Reduction Ship Utilizing the Euler-Euler Method

*Qidi Gao<sup>1</sup>, Wentao Wang<sup>1,2</sup>, Jianhua Wang<sup>1</sup>, Decheng Wan<sup>1\*</sup>*

<sup>1</sup> Computational Marine Hydrodynamics Lab (CMHL), School of Naval Architecture, Ocean and Civil Engineering, Shanghai Jiao Tong University, Shanghai, China

<sup>2</sup> China Ship Scientific Research Center, Wuxi, China

\*Corresponding author

### ABSTRACT

Air-layer drag reduction is a highly efficient and low-energy-consuming ship drag reduction method. It involves complex air-liquid two-phase flow, making it hard to obtain quantitative flow field data through model tests but numerical simulation can address this issue. However, accurately simulating such complex flow is challenging. This study focuses on numerical simulation methods for air-layer drag reduction ships. By using the Euler-Euler two-fluid method on the OpenFOAM platform, a numerical simulation is carried out for a specially designed VLCC ship model with a bottom air-layer device using the air-layer drag reduction method. The method can simulate air injection from the ship bottom to form a two-phase flow, as well as the air-layer and water-air mixed flow development. From the results, it can be summed up that the Euler-Euler method can well simulate the air-liquid two-phase flow at the bottom, with good accuracy for air-layer formation, mixing, evolution and diffusion. This method is of great significance for the numerical simulation of such air-layer drag reduction ships.

**KEY WORDS:** Air Drag Reduction; Numerical Simulation; Euler-Euler Method; Air-Liquid Flow.

### INTRODUCTION

Energy conservation and drag reduction are perennially significant objectives in the shipping industry. Firstly, reducing resistance is a crucial approach to lowering the operational costs of ships. For large transport vessels, the engine power generated from fuel consumption is primarily used to overcome the navigational resistance and maintain the forward motion of ship at a certain speed. Fuel costs account for a substantial proportion of the total operational costs of a ship, and fuel savings are of great importance in reducing these costs. By reducing the resistance of a ship, the engine power required to maintain its speed can be decreased, thereby achieving the effect of saving fuel and improving efficiency.

For various methods of ship drag reduction, the air-layer drag reduction method is a new method of ship drag reduction this year, and the feasibility of this technology has been verified on some experimental ships. The fundamental concept of air-layer drag reduction is injecting an appropriate amount of air from the bottom of the ship. With the auxiliary function of gas cavity structures such as side plates and bow and stern blocks, the air is retained within the cavities, forming a

complete air layer of a certain thickness. This air layer completely separates the ship's bottom surface from the water, effectively reducing the wetted surface area of the vessel, thereby achieving the goal of reducing frictional resistance. At present, a few countries such as the Netherlands, Japan and the United States have achieved preliminary demonstration applications. Including the gas drag reduction system (ACS) developed by the Dutch DK Group company, gas drag reduction system (ALS) developed by Mitsubishi Heavy Industries, Japan (Mizokami, et al, 2010; Kawabuchi, et al, 2011; Kawakita, et al, 2013), and its application in Yamatai ocean transport ship (Makiharju, et al, 2012; Hoang, et al, 2009). More and more experimental studies have shown that the air-layer drag reduction technology has a significant effect on reducing ship resistance.

At present, the research on the air-layer drag reduction mainly includes experimental and numerical simulation methods. The experiment mainly has the axisymmetric body experiment (Michael, et al, 1973) and plate experiment (Pal et al, 1988; Merkle et al, 1992). In these experimental studies, the drag reduction effect of bubbles or air-layer has been verified. At the same time, the factors affecting the drag reduction effect, such as bubble size, air rate and injection position, are also analyzed (Gao, et al, 2023). In addition, various ship model experiments have also verified the drag reduction effect of air-layer drag reduction. However, due to the complex two-phase flow in the drag reduction of bubbles or air-layer, as well as the deformation and coalescence of bubbles, it is difficult to obtain quantitative experimental data such as near-wall porosity, gas coverage area, gas layer thickness and so on. In order to change a variable such as the injection position in the experiment for different working conditions, the model needs to be adjusted or remade, which leads to a large error and low repeatability of the experiment, making it difficult to study the drag reduction problem of the air-layer through physical experiments. And numerical simulation can solve this problem well.

Air-Liquid flow is a typical continuous liquid-discrete gas coupled two-phase flow. Considering its complexity, it is difficult to directly solve the large-scale discrete bubbles contained in it based on grids. Therefore, it is necessary to establish mathematical models for microbubbles and continuous liquid flow respectively (Sundaresan, et al, 2018). The numerical simulation methods for such problems can be divided into Euler-Euler method and Euler-Lagrange method according to the description of discrete phase. For the numerical simulation of large scale such as model scale or full scale, the Euler-Lagrange method requires a lot of calculation. It is difficult to achieve in practice, so it is appropriate to use the Euler-Euler method. The Euler-Euler method establishes the governing equations for the liquid phase and the gas phase respectively,

and uses the phase fraction  $\phi$  as the data transmission medium to solve the two-phase flow problem, and This method has been widely applied to the industrial simulation of some bubble plume problems (Elena Díaz, et al, 2008). The coupling between the continuous phase and the discrete phase is realized by the force source term, which also includes drag force, lift force, virtual mass force, fluid inertia force and other models (Schiller, et al, 1935; Ishii, et al, 1979; Tomiyama, et al, 2004). In the early research, the accuracy of the method was verified by the problems of one-dimensional air-liquid boundary layer, two-dimensional flat bubble drag reduction and three-dimensional hydrofoil bubble drag reduction, and good accuracy results were obtained (Kunz, et al, 2003; Skudarnov, et al, 2006). For complex bubble kinematics problems such as bubble coalescence and breakup, the Population Balance Model (PBM) can be introduced to solve them (Hulburt, et al, 1964). Mohanarangam (2009) simulated the drag reduction process of turbulent boundary layer with bubbles based on the Euler-Euler method. The breakup and coalescence of bubbles are considered based on the PBM and the results are in good agreement with the experimental results (Xiang, et al, 2011). In this study, the numerical simulation of air-layer drag reduction is carried out for a specially designed VLCC model scale ship model with air drag reduction devices. Based on the Euler-Euler method, using the open source CFD platform OpenFOAM, process of jetting air from the bottom of the ship to the water to form an air-liquid mixed flow is simulated. At the same time, the flow condition of air-liquid mixed flow in the boundary layer at the bottom of the ship, the flow development process of air-liquid mixed flow and the evolution and development process of air layer are concerned.

## NUMERICAL METHODS

### Governing Equations

The governing equations of the Euler-Euler two-fluid model consist of the following two-phase continuity equations and momentum equations:

$$\frac{\partial(\alpha_\phi \rho_\phi)}{\partial t} + \nabla \cdot (\alpha_\phi \rho_\phi U_\phi) = 0 \quad (1)$$

$$\frac{\partial(\alpha_\phi \rho_\phi U_\phi)}{\partial t} + \nabla \cdot (\alpha_\phi \rho_\phi U_\phi U_\phi) + \nabla \cdot (\alpha_\phi \tau_\phi) + \nabla \cdot (\alpha_\phi \rho_\phi R_\phi) = -\alpha_\phi \nabla p + \alpha_\phi \rho_\phi g + M_\phi \quad (2)$$

The subscripts of each parameter  $\phi = a, b$  in the formula represent the dispersed phase and the continuous phase,  $\tau_\phi$  is the viscous stress term,  $R_\phi$  is the Reynolds stress term,  $M_\phi$  is the interphase force, and  $U_\phi$  is the velocity of each phase, respectively. The above equation is a conserved form, but the result obtained by solving the equation is the momentum value of each time step. If the solution speed is required, the momentum value needs to be divided by the product of the volume fraction  $(\alpha_\phi \rho_\phi U_\phi) / \alpha_\phi \rho_\phi$ . when the phase fraction of the discrete phase is small, that  $\alpha_\phi$  is 0, the method will have numerical errors, so the equation needs to be improved. This problem is solved by constructing a ‘‘Phase-Intensive’’ momentum equation. The form is as follows:

$$\frac{\partial(\alpha_\phi \rho_\phi U_\phi)}{\partial t} = \alpha_\phi \rho_\phi \frac{\partial(U_\phi)}{\partial t} + U_\phi \frac{\partial(\alpha_\phi \rho_\phi)}{\partial t} \quad (3)$$

$$\nabla \cdot (\alpha_\phi \rho_\phi U_\phi U_\phi) = \alpha_\phi \rho_\phi U_\phi \cdot \nabla(U_\phi) + U_\phi \nabla \cdot (\alpha_\phi \rho_\phi U_\phi) \quad (4)$$

The left and right sides of the above formula are added and the improved equation is obtained:

$$\frac{\partial(\alpha_\phi \rho_\phi U_\phi)}{\partial t} + \nabla \cdot (\alpha_\phi \rho_\phi U_\phi U_\phi) = \alpha_\phi \rho_\phi \left[ \frac{\partial(U_\phi)}{\partial t} + U_\phi \cdot \nabla(U_\phi) \right] + U_\phi \left[ \frac{\partial(\alpha_\phi \rho_\phi)}{\partial t} + \nabla \cdot (\alpha_\phi \rho_\phi U_\phi) \right] \quad (5)$$

The second bracket at the right end of the above equation is the continuity equation (1), and its value is 0, so the equation is obtained:

$$\frac{\partial(\alpha_\phi \rho_\phi U_\phi)}{\partial t} + \nabla \cdot (\alpha_\phi \rho_\phi U_\phi U_\phi) = \alpha_\phi \rho_\phi \left[ \frac{\partial(U_\phi)}{\partial t} + U_\phi \cdot \nabla(U_\phi) \right] \quad (6)$$

The right side of the above equation is replaced by the first term on the left side of equation (2), and the final momentum equation is obtained. The viscous stress term and the Reynolds stress term can be expressed as follows:

$$\nabla \cdot (\alpha_\phi \tau_\phi) + \nabla \cdot (\alpha_\phi \rho_\phi R_\phi) = \nabla \cdot [\alpha_\phi \rho_\phi R_{eff,\phi}] \quad (7)$$

Where the  $R_{eff,\phi}$  is combined form of viscous stress and Reynolds stress, which is expressed by the following formula:

$$R_{eff,\phi} = -\nu_{eff} [\nabla U_\phi + \nabla^T U_\phi] + \frac{2}{3} \nu_{eff} (\nabla \cdot U_\phi) \mathbf{I} + \frac{2}{3} k_\phi \mathbf{I} - \nu_{eff} \nabla U_\phi + R_{c,\phi} \quad (8)$$

Where  $R_{c,\phi}$  is:

$$R_{c,\phi} = -\nu_{eff} \nabla U_\phi^T + \frac{2}{3} \nu_{eff} (\nabla \cdot U_\phi) \mathbf{I} + \frac{2}{3} k_\phi \mathbf{I} \quad (9)$$

If the compressibility of the fluid is not considered, that is, the density is constant, the incompressible Euler-Euler two-fluid model equations can be obtained as follow:

$$\frac{\partial(\alpha_\phi)}{\partial t} + \nabla \cdot (\alpha_\phi U_\phi) = 0 \quad (10)$$

$$\frac{\partial U_\phi}{\partial t} + U_\phi \cdot \nabla U_\phi - \nabla \cdot [\nu_{eff} \nabla U_\phi] + \nabla \cdot [R_{c,\phi}] + \frac{\nabla(\alpha_\phi)}{\alpha_\phi} \cdot [-\nu_{eff} \nabla U_\phi + R_{c,\phi}] = -\frac{\nabla p}{\rho_\phi} + g + \frac{M_a}{\alpha_\phi \rho_\phi} \quad (11)$$

### Turbulence Model

The turbulence model used in the Euler-Euler two-fluid solution adopts the large eddy simulation (LES) model. The motion is divided into two categories: large-scale and small-scale vortices by filtering. The large-scale is calculated directly, and the small-scale is solved by modeling. The filtering operation is as follows:

$$\bar{\phi}(x, t) = [G(r, x) \phi(x - r, t)] dr \quad (12)$$

Where  $\phi(x - r, t)$  is the filtered variable and  $G(r, x)$  is the filtered function. The N-S equation is obtained by filtering as follows:

$$\frac{\partial \bar{U}_j}{\partial t} + \frac{\partial \bar{U}_i \bar{U}_j}{\partial x_i} = \nu \frac{\partial}{\partial x_i} \left( \frac{\bar{U}_j}{\partial x_i} \right) - \frac{1}{\rho} \frac{\partial \bar{p}}{\partial x_j} - \frac{\partial}{\partial x_i} \tau_{ij}^R \quad (13)$$

Among them, the  $\tau_{ij}^R$  term represents the residual stress, which is an unknown term and will cause the equation to be not closed. The equation is solved by the Smagorinsky model, as follows:

$$\tau_{ij}^R \equiv -2(C_S \Delta)^2 |\bar{S}| \bar{S}_{ij} + \frac{2}{3} k_r \delta_{ij} \quad (14)$$

Where  $C_S$  is the Smagorinsky coefficient, which is a fixed value in the whole basin;  $\bar{S}_{ij}$  is the deformation rate tensor of the solvable scale, and  $|\bar{S}|$  is the size of the deformation rate tensor, which are calculated by the following equations :

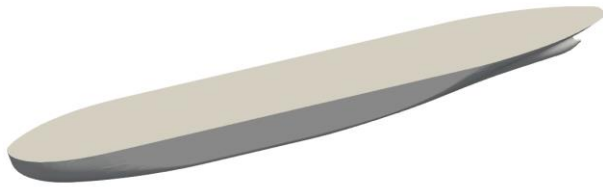
$$\bar{S}_{ij} = \frac{1}{2} \left( \frac{\partial U_i}{\partial x_j} + \frac{\partial U_j}{\partial x_i} \right) \quad (15)$$

$$|\bar{S}| = \sqrt{2 \bar{S}_{ij} \bar{S}_{ij}}$$

## SIMULATION CASES

### Model Scale Ship Model

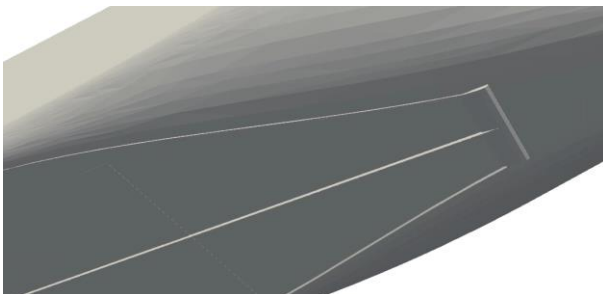
The ship model selected in this research is a KVLCC ship model, which has been specially designed and installed with an air-layer drag reduction device at the bottom. Through the air-layer device, the gas can form a gas layer with a certain thickness in a certain range of the bottom of the ship, which is shown in Fig. 1.



(a) KVLCC ship model



(b) Bow air-layer device



(c) Stern air-layer device

Fig. 1 Specially designed KVLCC ship model with air-layer devices

In this study, the total length of the KVLCC ship model is 7 m, the draught is 0.4295 m, and the experimental speed is 1.117 m/s. There are three rows of injection air holes at the bottom of the ship, and the air-liquid mixed flow is formed and the air layer is formed by continuous injection. The air holes is shown in Fig. 2.

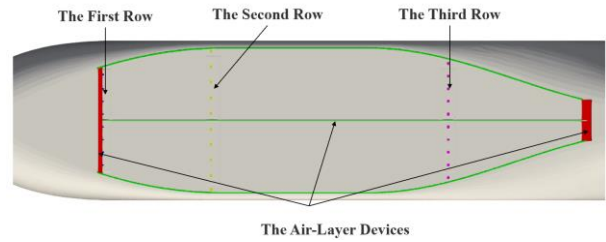


Fig. 2 Bottom air holes setting

Among them, the size of all the air holes is 1 cm, the number of air holes in first row is 8, the second row is 12, the third row is 10, and the air holes in each row are evenly spaced.

### Computational Domain and Mesh

In this research, the numerical simulation of the ship model only considers the two-phase flow involved in the drag reduction process of the air-layer, without considering the two-phase flow of the free surface. Therefore, in the numerical simulation, the method of overlapping mode is adopted, that is, the calculation area of the hull is taken from the water line without considering the hull part and air above the water line. The length of the computational domain is 4 times the length of the ship, the bow to the entrance of the computational domain is once the length of the ship, and the stern to the exit of the computational domain is twice the length of the ship. The width and depth of the calculation domain are once the length of the ship, which is shown in Fig. 3. The left boundary of the computational domain is an inlet with uniform inflow. The left, right, top and bottom boundaries are symmetric boundary conditions. The right boundary is an outlet with a fixed velocity of zero.

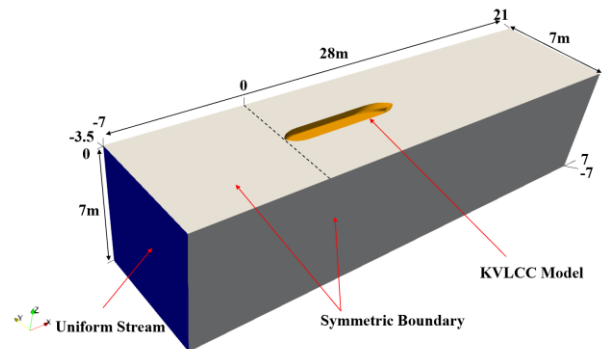


Fig. 3 The calculation domain setting

Because the numerical simulation of two-phase flow requires more fine meshing, and in order to reduce the total number of grids as much as possible, the grid refinement near the hull is used for meshing, as shown in Fig. 4.

The total number of grids used in the numerical simulation is about 12.5 million, and the air layer device at the bottom of the hull is separately refined. For the numerical simulation of the air holes in the experiment, by setting the generated part of the hull surface corresponding to the position of each air holes as a special inlet boundary, the gas is injected into the water. The air hole mesh is shown in Fig. 5.

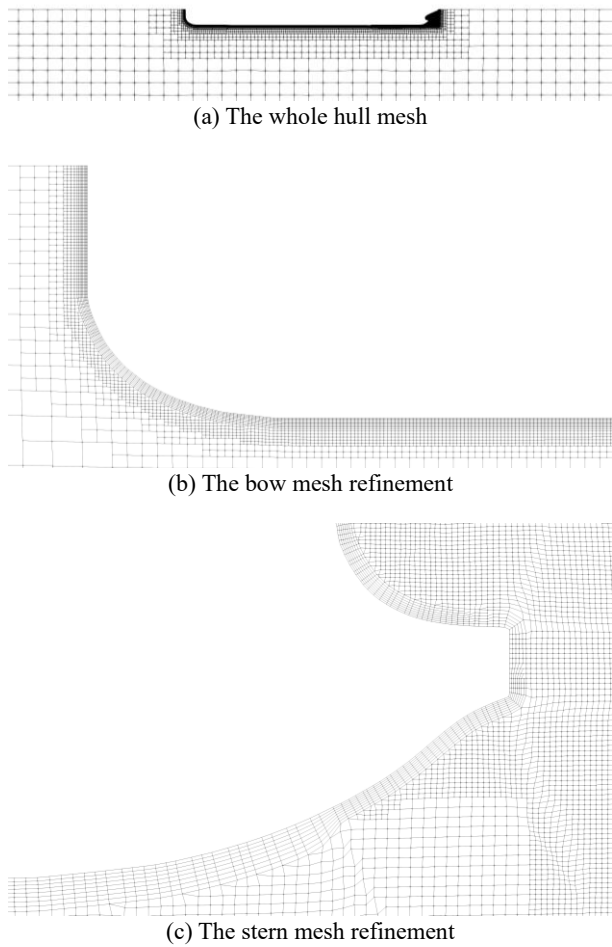


Fig. 4 Hull mesh and boundary layer mesh refinement

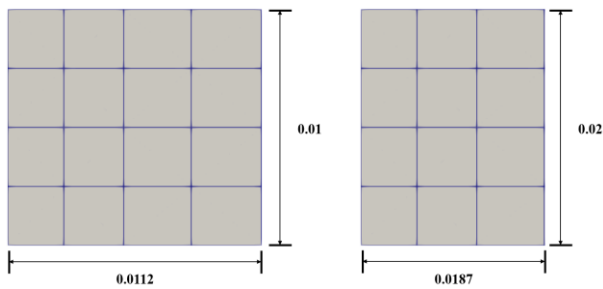


Fig. 5 The mesh of air holes (the left is the first row of holes, and the right is the second and third rows of holes)

In the numerical simulation, the air injection velocity required in the numerical simulation is obtained by combining the injection volume of each hole in the experiment and converting the size of the hole mesh with the size of the real circular holes. The injection volume of each air hole in the experiment and the injection volume in the numerical simulation are shown in Table. 1.

Table 1. The injection volume of each row in numerical simulation

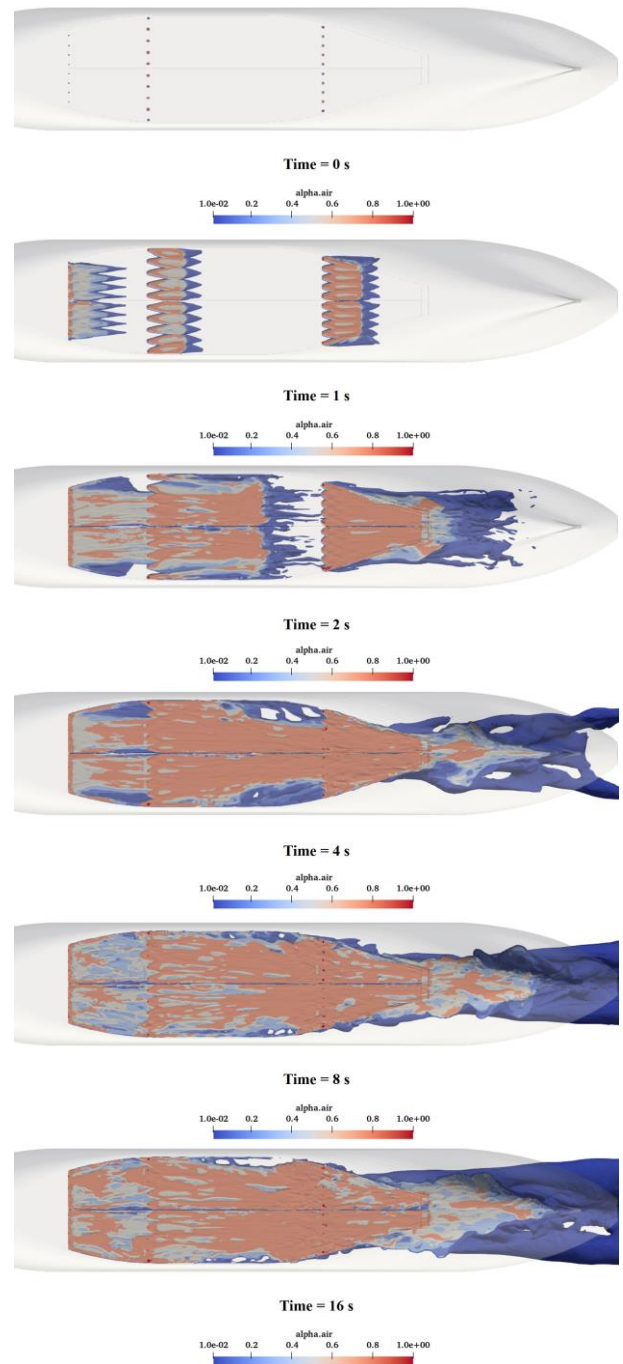
Term	Row 1	Row 2	Row 3
Injection volume in the experiment	157 L/min	145 L/min	134 L/min
Total size of air holes in numerical simulation	8.96 cm <sup>2</sup>	44.88 cm <sup>2</sup>	37.4 cm <sup>2</sup>
The injection velocity in numerical simulation	1.915 m/s	0.5347 m/s	0.8377 m/s

In the numerical simulation, according to the total size of the computational domain and the even inflow velocity, a total computing time of 20 s is calculated to stabilize the flow field in the computational domain. At the same time, the air-liquid mixing can reach a stable state. The calculation time step is 0.0001 seconds. This setting can ensure that the Courant number is about 1, so that the calculation is not easy to diverge, and can ensure the accuracy of the calculation results.

## RESULTS AND DISCUSSION

### Air-Liquid Mixed Flow Field

Figure 6 shows the air phase fraction at the bottom of the ship in 0 to 20 seconds. From the initial time of calculation to the calculation of 1 s, the three rows of holes can normally inject air, and move backward with the flow direction. The gas diffuses to both sides after injection, and fuses with the air of other holes to form a whole air layer.



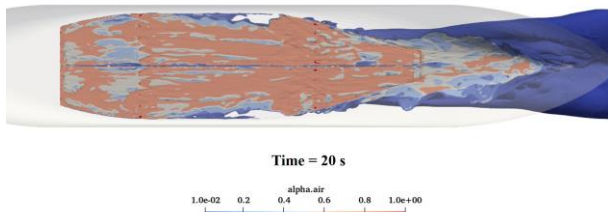


Fig. 6 The air fraction at the bottom of the ship when time is 0 to 20 s

When the calculation time reaches 2 s, the air injected from the first row has flowed to the second row, and the air injected from the third row of holes has flowed through the tail air-layer device to the tail of the ship and began to float. When the calculation time reaches 4 s, the air layer at the bottom of the ship has basically developed, and the air layer formed by the first two rows of holes has flowed to the third row of holes. At the same time, under the action of the air-layer device on both sides of the bottom of the ship, the gas is limited to diffuse from both sides, so that the obvious boundary between the gas and the air-layer device can be seen, so that the air inside the air-layer device continues to accumulate to form a thicker air layer. When the calculation time reaches 8 s, the development of the air layer at the bottom of the ship is basically stable, and the thickness of the air layer at each position basically maintains a dynamic balance. The excess air flows out of the bottom area of the ship through the air-layer device at the stern of the ship, and floats along the ship wall from both sides of the stern under the action of buoyancy. Another part of the air with low phase fraction (actually tiny bubbles) will continue to flow backward and float slowly when leaving the stern of the ship due to its small influence of buoyancy, forming a small air-phase mixed flow area dispersed in a certain range of the stern flow area. Figure 7 shows the air fraction at the bottom of the ship when the calculation time is 0 to 20 s. The evolution of the air phase fraction contour with time is basically the same as that of Fig. 6. When the air fraction threshold is adjusted to 0.01, a large number of air fraction contour surface can be seen at the stern of the ship.

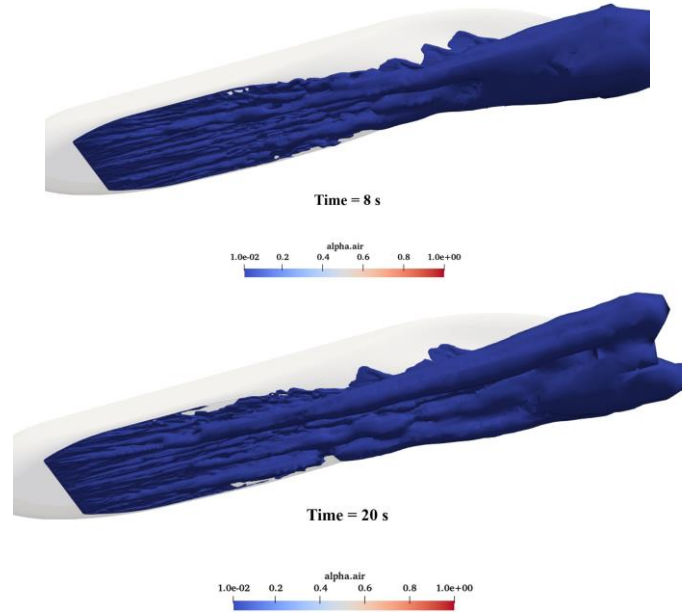


Fig. 7 Low air fraction distribution at the bottom of the ship when time is 0 to 20 s

Since the air fraction threshold set in the figure 7 is low (0.01), a large number of air fraction contours are shown at the stern of the ship, which can be understood as some microbubbles generated by the previous mixed flow in the actual experiment. Because of its small bubble size, the effect of buoyancy on bubbles is much smaller than that of water flow, so it can move with the flow for a long distance, forming the stern air cloud area.

It can be seen from the Fig. 8 that when the air fraction threshold is set to 0.5, the air layer state near the wall at the bottom of the ship can be relatively clearly displayed. The air at the bottom of the ship is mainly concentrated in the inner side of the air-layer device and forms a continuous air layer. A small amount of air overflows from both sides of the hull. Most of the flowing air has basically diffused when it flows to the stern of the ship, and only a small part of the air will move to the vicinity of the stern propeller.

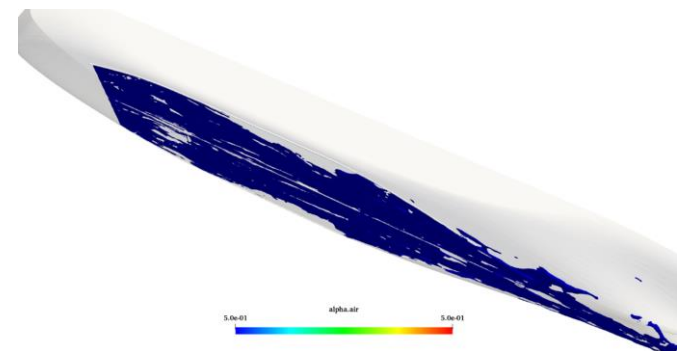
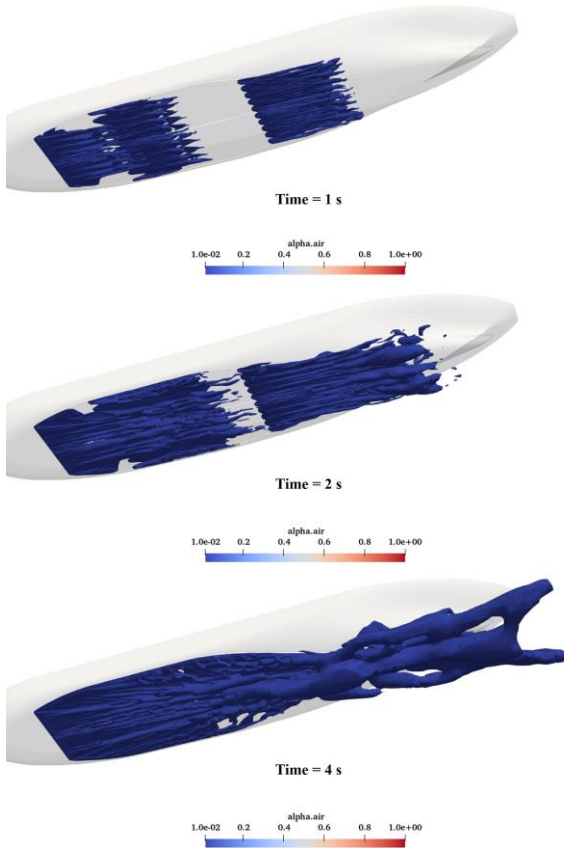


Fig. 8 Air layer distribution at the bottom of the ship when time is 20 s

Due to the effect of the air-layer device at the bottom and tail of the ship, when the air (a large number of microbubbles) in the air-liquid mixed flow flows to the stern, it will quickly move upward from the stern along the sides of the ship under the action of buoyancy, as shown in Fig. 9. A small number of microbubbles (low air fraction) will continue to move backward with the flow under the action of air-liquid mixed flow, leaving the air-layer device to reach the flow field of the propeller.

## Air Fraction in Air-Liquid Flow

Figure 10 shows the distribution of air phase fraction along the flow direction from the maximum width of the tail device to the position of the first row of air holes within the range of drag reduction device at the bottom of the ship. The test line is 0.153 m away from the symmetry axis of the ship, and the distance between the test line and the bottom of the ship is 0.5 cm. The data of four moments: time= 4 s, 8 s, 16 s and 20 s were selected for comparison. For each group of data, a total of 5 time steps before and after the data were selected for average processing.

From the Fig. 10, it can be seen that the temporal and spatial distribution of the air fraction at the bottom of the ship is roughly the same, indicating that the air-liquid mixing process has been basically completed from 8 s, and the air-liquid mixing flow gradually tends to be stable. At this time, the air phase fraction in the two-phase flow does not change much. However, it can be seen that with the increase of time, the high air fraction area at the rear of the ship gradually moves forward. The reason for this phenomenon is that due to the effect of the air-layer device, all air have a tend to converge at the tail of the ship. At this time, the air in the two-phase flow from the front to the tail will gradually accumulate at the tail to form a continuous air layer. When the thickness of the air layer reaches the designed threshold, the excess air will overflow from the rear side of the air-layer device, so that the thickness and coverage area of the inner air layer of the air-layer device remain dynamically balanced.

Figure 11 shows the spatial distribution of the air fraction at the bottom of the ship at three different test positions at time is 20 s. The three test positions are 0.0387 m, 0.153 m, and 0.385 m from the ship symmetry axis, respectively.

Where line 2 is the position tested in Figure 10. The third test position is the widest position of the air-layer device. For each group of data, a total of 5 time steps before and after the data were selected for average processing.

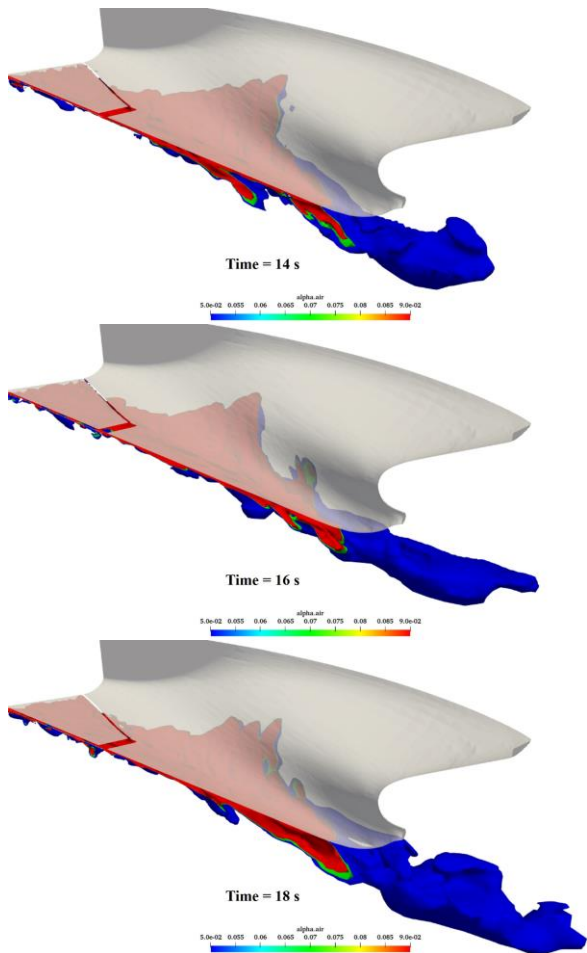


Fig. 9 Air phase fraction contour of stern when time is 14, 16 and 18 s

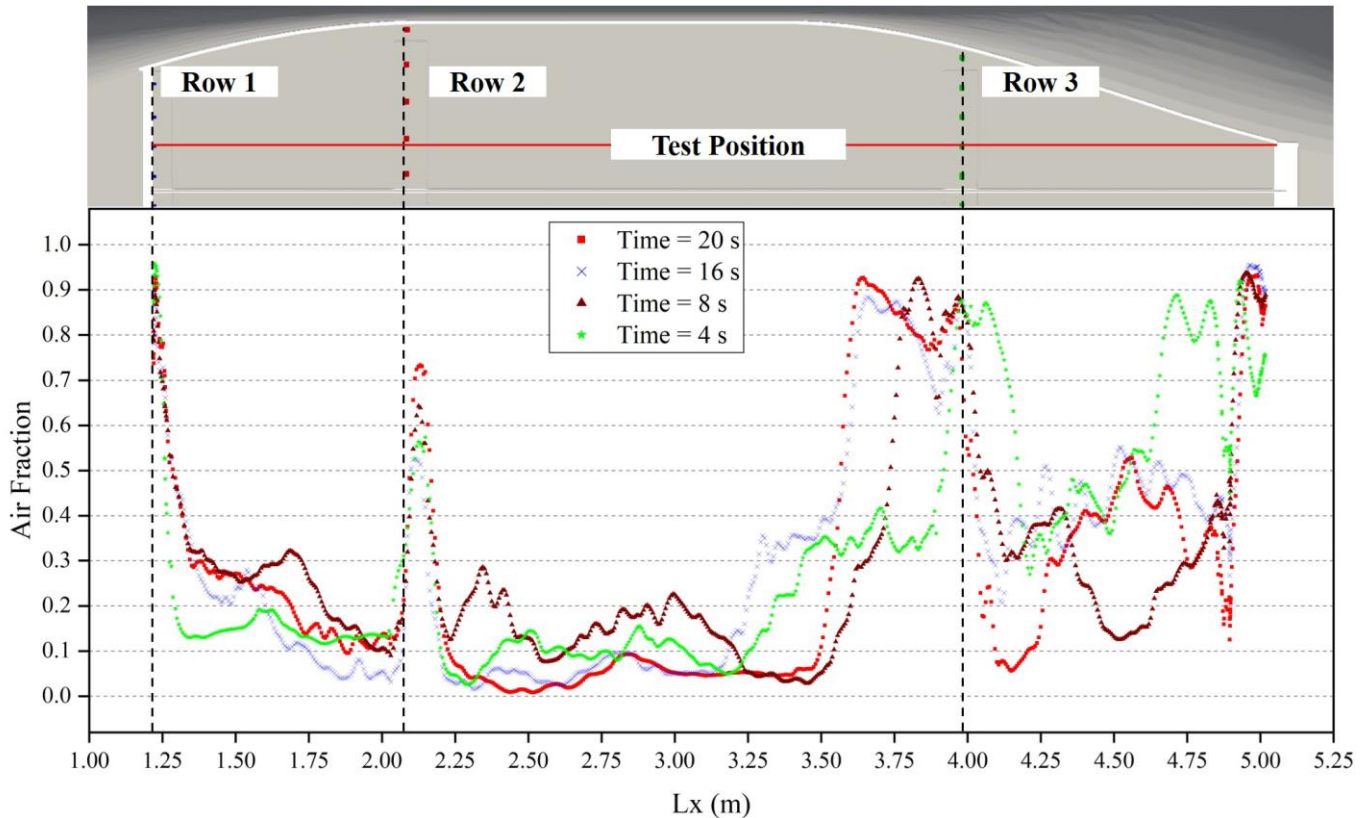


Fig. 10 The spatial distribution of air fraction along the flow direction at different times of ship bottom

From the Fig. 11, it can be seen that in the case that the air-liquid mixed flow has been fully developed, the air fraction at the three locations has a similar spatial distribution. However, through regional comparison, it is found that the air phase distribution of the three is different. Between the first row and the second row of air holes, the air fraction at line 3 is smaller, while the air fraction at line 1 near the outside is higher. The reason is that the air has a tend to diffuse to both sides during the flow movement, so the air at the bottom of the ship has a tend to diffuse to

both sides of the ship from the beginning of the injection. From the second row to the third row of holes, because the previous air has accumulated, and under the action of the air layer devices on both sides, the trend of air diffusion in the mixed flow is suppressed. Therefore, at this stage, the air phase fraction distribution at the three test positions is basically the same. When the mixed flow reaches the stern of the ship through the third row of air holes, the air has gradually accumulated and

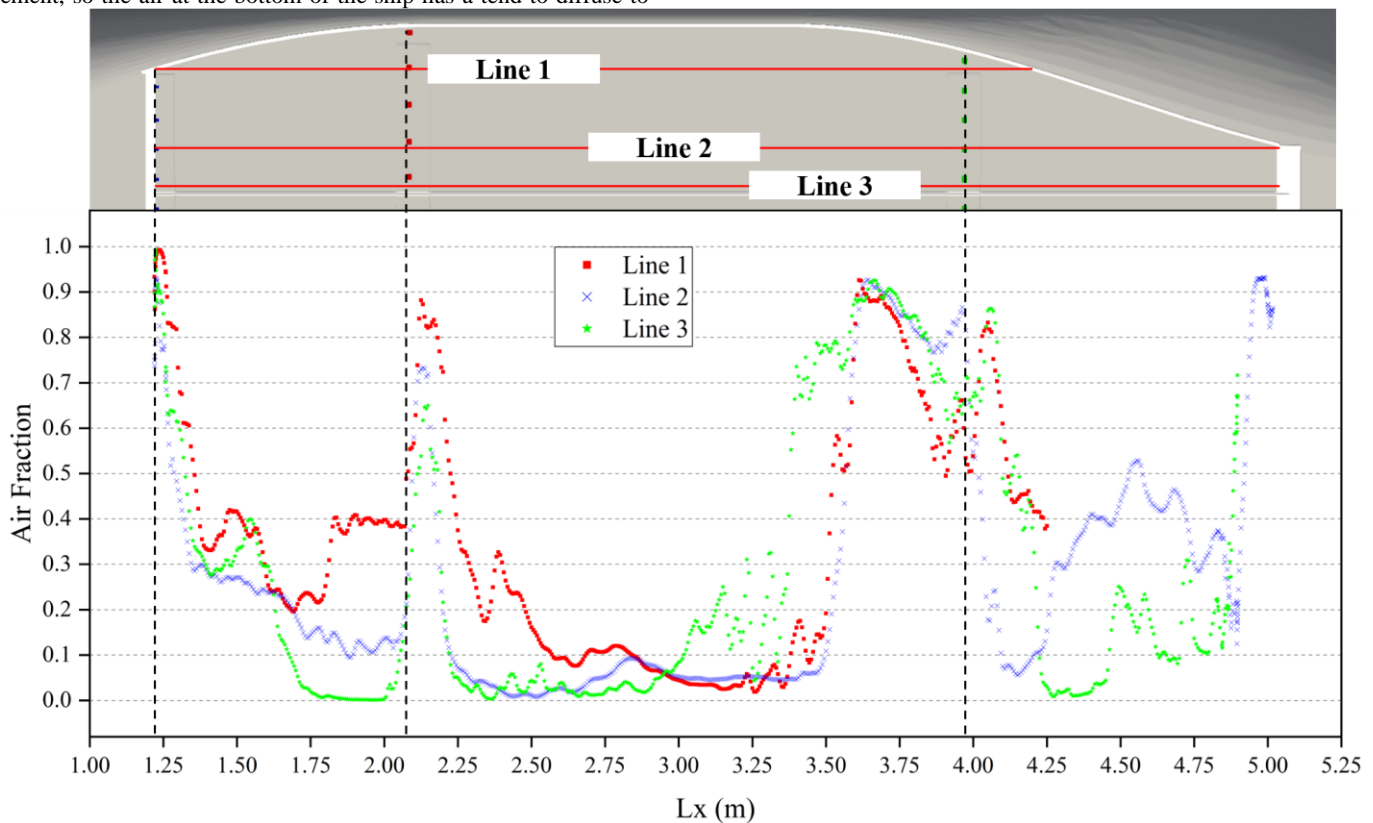


Fig. 11 The spatial distribution of air fraction along the flow direction at different test positions when time is 20 s

formed a continuous air layer under the action of the air layer device. Therefore, in this part, the air fraction of the three test positions is generally higher. Due to the air accumulation effect of the air-layer device, the air fraction at line 2 and line 3 near the middle of the ship is higher. At this time, it can be considered that a relatively continuous thin air layer can be formed after the third row of air holes.

## CONCLUSIONS

In this paper, a numerical simulation study is carried out for a specially designed VLCC ship equipped with an air-layer drag reduction device. For the complex air-liquid mixed flow, the Euler-Euler two-fluid model is used as the basic method of numerical simulation to study the air-liquid mixed flow of the air-layer drag reduction ship, and the following conclusions are obtained:

The Euler-Euler two-fluid model can better simulate the air-liquid mixed flow at a large scale, including the injection of air into the liquid and the formation of mixed two-phase flow, as well as the flow process of mixed flow along the wall. At the same time, it can better simulate the motion state of air under the action of liquid in the mixed flow. Although the capture of the bubble boundary cannot be achieved, the complex interaction between the two phases can also be achieved by increasing the interphase force model.

Through the numerical simulation of the experimental conditions, it is found that the simulation results of the numerical simulation are similar to the experimental results. The temporal and spatial

distribution of the air fraction at different positions at the bottom of the ship is analyzed, and it is found that due to the diffusion of air in the fluid, the air in the mixed flow always has a tend to diffuse along the direction perpendicular to the flow direction. The air fraction in the mixed flow decreases rapidly after leaving the air hole, and the air fraction on both sides behind the hole increases gradually and reaches a state of dynamic equilibrium. Under the action of the air-layer device, the air in the mixed flow cannot diffuse from the bottom of the ship to both sides, and as the device gathers at the stern of the ship, the air in the two-phase flow further accumulates at the stern of the ship and gradually forms a continuous air layer. From the numerical simulation results, it can be seen that when the air-liquid mixed flow reaches a stable state, the continuous air layer coverage at the stern of the ship can basically reach the position of the third air hole, thus producing a certain drag reduction effect.

## ACKNOWLEDGEMENT

This work is supported by the National Natural Science Foundation of China (52131102), to which the authors are most grateful.

## REFERENCES

Elena Díaz, M, Iranzo, A, Cuadra, D, et al (2008). "Numerical simulation of the air-liquid flow in a laboratory scale bubble column: Influence of

- bubble size distribution and non-drag forces,” *Chemical Engineering Journal*, 139(2), 363-379.
- Hoang, CL, Toda, Y, Sanada, Y (2009). “Full scale experiment for frictional resistance reduction using air lubrication method,” *Proc 19th Int Offshore and Polar Eng Conf*, Osaka, ISOPE, 3, 812-817.
- Hulburt, HM, Katz, S (1964). “Some problems in particle technology-a statistical mechanical formulation,” *Chemical Engineering Science*, 19(8), 555-574.
- Ishii, M (1979). “Drag coefficient and relative velocity in bubbly, droplet or particulate flows,” *A.I.Ch.E. Journal*, 25, 843-855.
- Kawabuchi, M, Kawakita, C, Mizokami, S, et al. (2011). “CFD predictions of bubbly flow around an energy-saving ship with mitsubishi air brication system,” *Mitsubishi Heavy Industries Technical Review*, 48(1), 53-57.
- Kawakita, C (2013). “Study on marine propeller running in bubbly flow,” *Proc 3th Int Symposium on Marine Propulsors*, Tasmania, 2013.
- Kunz, RF, Deutsch, S, Lindau, JW (2003). “Two fluid modeling of microbubble turbulent drag reduction,” *Proc 4th ASME-JSME Joint Fluids Engineering Conference*, Hawaii, 2003, 1-10.
- Makiharju, S., Ceccio, SL (2012). “Air lubrication drag reduction on great lakes ships,” *Great Lakes Maritime Research Institute*, 2012.
- Merkle, C (1992). “Drag reduction in liquid boundary layers by air injection,” *Prog. Astronaut. Aeronaut*, 123, 351-412.
- Michael, E, McCormick and Rameswar, B (1973). “Drag reduction of a submersible hull by electrolysis,” *Journal of Naval Engineers*, 85(2), 11-16.
- Mizokami, S, Kawakita, C, Kodan, Y, et al. (2010). “Experimental study of air lubrication method and verification of effects on actual hull by means of sea trial,” *Mitsubishi Heavy Industries Technical Review*, 47(3), 41-47.
- Mohanarangam, K, Cheung, SCP, Tu, JY, et al (2009). “Numerical simulation of micro-bubble drag reduction using population balance model,” *Ocean Engineering*, 36, 863-872.
- Pal, S, Merkle, CL, and Deutsch, S (1988). “Bubble characteristics and trajectories in a microbubble boundary layer,” *Physics of Fluids*, 31(4), 744-751.
- Schiller, L, Naumann, A (1935). “A drag coefficient correlation,” *V.D.I Zeitung*, 77, 318-320.
- Sundaresan, S, Ozel, A, Kolehmainen, J (2018). “Toward constitutive models for momentum, species, and energy transport in air-particle flows,” *Annual Review of Chemical and Biomolecular Engineering*, 9(1), 61-81.
- Tomiyama, A (2004). “Drag lift and virtual mass forces acting on a single bubble,” *Proc 3th Int Symposium on Two-phase Flow Modeling and Experimentation*, 2004, 22-24.
- Xiang, M, Cheung, SCP, Tu, JY, et al (2011). “Numerical research on drag reduction by ventilated partial cavity based on two-fluid model,” *Ocean Engineering*, 38, 2023-2032.